AIAA JOURNAL
Vol. 38, No. 2, February 2000

Inverse Aeroacoustic Problem for a Rectangular Wing

Trevor H. Wood* and Sheryl M. Grace†
Boston University, Boston, Massachusetts 02215

An investigation is made of the feasibility of aeroacoustic inversion, where the pressure on a thin, flat, rigid rectangular wing undergoing rigid oscillations or interacting with unsteady, subsonic flow is to be predicted from the far-field acoustic signal. This problem is ill-posed because small pressure fluctuations in the far field are larger in the near field by a factor equal to the reciprocal of the distance from the wing. In the inverse model, this ill-posedness manifests itself in the kernel of a two-dimensional Fredholm integral equation of the first kind. Discretization of this integral equation using a physically meaningful collocation series results in an ill-conditioned system of equations which is solved using the singular value decomposition (SVD). The SVD generally requires regularization techniques to discard redundant or unphysical information. An algorithm is developed for optimally determining the near-field pressure without relying on a user-specified regularization parameter. Tests using numerically generated input data show the inversion is feasible and accurate for accurate input data. The inversion remains feasible when errors are introduced in the far-field measurements and the measurable parameters of the flow.

Nomenclature

A = kernel matrix
$\boldsymbol{a}$ = complex amplitude of gust
$B_{ln}, \boldsymbol{b}$ = coefficients of the collocation series
$\tilde{b}$ = dimensionless half-span length in Prandtl–Glauert space
c = chord length
c_0 = ambient speed of sound
$\boldsymbol{f}$ = pseudoinverse coefficients
$G(\boldsymbol{x})$ = Green's function, $\exp(-iK_1|\boldsymbol{x}|)/|\boldsymbol{x}|$
J_n = Bessel function, order n, of the first kind
K_1 = Helmholtz wave number, Mk_1/β^2
k_1 = reduced frequency or Strouhal number, $c\omega/2U_0$
k_3 = spanwise wave number component
L, N = truncation indices for collocation series
M = freestream Mach number, U_0/c_0
$P(\tilde{\boldsymbol{x}})$ = complex pressure in Prandtl–Glauert space with $\exp(iMK_1\tilde{x}_1)$ transformation
$\boldsymbol{p}$ = vector of far-field measurements
r = rank of kernel matrix
$\hat{\boldsymbol{r}}$ = unit vector
S = diagonal matrix of nonzero singular values
$\mathcal{S}(k_1)$ = Sears function
t = time scaled by $c/2U_0$
U_0 = freestream fluid velocity
$\boldsymbol{u}_i, U$ = left singular vectors, matrix
$\boldsymbol{v}_i, V$ = right singular vectors, matrix
$\boldsymbol{x}$ = space scaled by $c/2$
$\tilde{\boldsymbol{x}}$ = Prandtl–Glauert coordinates
β = Prandtl–Glauert parameter
γ = acoustic cutoff parameter
ΔP = pressure jump across wing
θ = transformed streamwise coordinate, $\cos^{-1}(-\tilde{y}_1)$
ϑ = declination angle
ρ_0 = ambient fluid density
Σ = matrix of singular values
σ_i = singular values
τ = regularization parameter
ϕ = transformed spanwise coordinate, $\cos^{-1}(-\tilde{y}_3/\tilde{b})$
φ = azimuthal angle
ω = frequency of unsteady disturbance

Subscript

E = last element of vector

Superscripts

H = conjugate transpose of matrix
$+$ = pseudoinverse of matrix

Introduction

INTEREST in inverse problems has grown in recent years with the hope of increasing technological productivity by providing new and accurate methods for noninvasive sensing and design optimization. To determine the cause of a phenomenon using knowledge of a measured or desired effect is the goal of an inverse problem. In acoustics, for instance, the cause may be a vibrating body, and the effect is the acoustic radiation emanating into the surrounding medium. In the fields of aeroacoustics and hydroacoustics, inverse techniques may be used for many applications including the noise reduction of airframe components, nondestructive testing of turbomachinery, source detection, structural silencing, advanced propeller design, etc.

Two popular techniques for inverse acoustical analysis are acoustic holography[1–3] and phased arrays.[4–8] Researchers currently use acoustic holography as a tool for cabin and ship hull design because of its ability to quantify the structural–acoustic coupling between the fluid loaded structures and adjacent interior spaces.[2] Acoustic holography determines the velocity and pressure fields on the surface of a vibrating body from measurements of the acoustic pressure in the surrounding medium. The technique, however, relies on acoustic radiation into a quiescent field, which is a limiting feature from the aeroacoustic perspective. Phased arrays, on the other hand, are usually used when either the field is in motion[4–7] or the sources of sound are in motion.[8,9] These techniques employ multiple microphones to measure the sound emanating from a chosen location and frequency. A greater number of microphones leads to greater resolution, at the expense of higher testing/setup costs. Phased arrays work well as a general inverse measurement technique when little is known about the source distribution being imaged. The inverse aeroacoustic techniques developed in this research, however, are for application to a particular problem of interest to the aeroacoustics and hydroacoustics community for which knowledge of the possible source distributions exists. By taking this knowledge into account, inverse solutions may be obtained in a more efficient manner.

Received 16 September 1998; revision received 14 June 1999; accepted for publication 9 July 1999.

*Graduate Research Assistant, Aerospace and Mechanical Engineering Department, 110 Cummington Street; twood@bu.edu. Student Member AIAA.

†Assistant Professor, Aerospace and Mechanical Engineering Department, 110 Cummington Street; sgrace@bu.edu. Member AIAA.

The inverse aeroacoustic problem involves the determination of the surface pressure of a radiating body from acoustic data in the surrounding fluid. The eventual long-term goal that prompted this research is to be able to measure the unsteady surface pressure loads on a rotating turbine/propeller blade noninvasively. This will only be realized through the systematic development of inverse solutions to simpler problems, as had been done for the direct problem.

The objective of the direct aeroacoustic problem is to calculate the far-field sound using the known surface forces produced by unsteady motion or flow disturbances. Historically, the first of such problems considered in aeroacoustics involved a thin, flat airfoil. The unsteady surface pressure distribution for the flat airfoil was known for both airfoil motion[10,11] and mean flow inhomogeneities including vortical inflow[12–16] and was used to calculate the far-field acoustics.[17–19] These classical results have since been extended to include the effects of transonic flow, airfoil geometry, three-dimensional effects, multiple lifting surfaces, rotating reference frame, etc.

The inverse aeroacoustic problem has been developed thus far in the same manner as the direct problem. The first inverse problem considered the simple rigid, flat airfoil[20,21]; recently, an extension for a flat wing was initiated.[22,23] It has been shown that, mathematically, the inverse problem is ill-posed because of possible nonuniqueness and because the solution is inherently unstable to errors in the input data. In Ref. 22, a plausible method for performing the inversion was presented; however, it was not robust even for very accurate input data from the acoustic field. The technique was refined to filter optimally the error using a systematic and robust approach, which is necessary to allow for a practical implementation of the method. Preliminary results using the modified method were presented in Ref. 23. This paper completes the study by fully describing the method and presenting the results from the sensitivity analysis.

The inverse technique for the three-dimensional flat wing is formulated using a linearized analysis that relates the far-field and near-field pressures through an integral equation. This relation is general for an ideal, laminar fluid flow regardless of what generated the surface pressure distribution aerodynamically, for example, gust interaction, incident acoustics, or airfoil oscillations. The integral equation is written into matrix form using the collocation method, where the choice of the collocation series allows for the inclusion of the known physics of the problem. Because the inverse problem is ill-posed, the resulting system of equations is ill-conditioned. The matrix equation is solved using the singular value decomposition (SVD) with regularization to remove the contribution of errors in the computation and the acoustic measurements. The regularization is achieved using a newly developed technique that yields good results for subcritical Mach numbers and reduced frequencies up to and including 0.8 and 7.0, respectively. The effect of measurement errors on the accuracy of the inverse solutions is also investigated, and the robustness of the method is shown.

Mathematical Formulation

In Refs. 21 and 22, it was shown that the response of a thin, flat, rigid wing to a weak unsteady vortical gust in a subsonic, high-Reynolds-number flow (Fig. 1) is characterized by a Helmholtz equation for a modified pressure (in Prandtl–Glauert and Reissner space). The same governing equation may be written for an acoustic disturbance interacting with the wing and for rigid oscillations of the wing in steady flow. The solution may be written in integral form as [Eq. (9) in Ref. 22]

$$P(\tilde{\boldsymbol{x}}) = -\frac{1}{4\pi}\int_{-\tilde{b}/2}^{\tilde{b}/2}\int_{-1}^{1} \Delta P(\boldsymbol{y})\left.\frac{\partial G(\tilde{\boldsymbol{x}}-\tilde{\boldsymbol{y}})}{\partial \tilde{y}_2}\right|_{\tilde{y}_2=0} \mathrm{d}\tilde{y}_1\,\mathrm{d}\tilde{y}_3 \qquad (1)$$

where $\Delta P(\boldsymbol{y}) = P(\tilde{y}_1, 0^+, \tilde{y}_3) - P(\tilde{y}_1, 0^-, \tilde{y}_3)$. All spatial variables are scaled with the half-chord length and the unsteady pressure is related to $P(\tilde{\boldsymbol{x}})$ by

$$p'(\tilde{\boldsymbol{x}}, t) = \rho_0 |a_2| U_0 \,\mathrm{Re}\left\{\frac{1}{2\pi}\int_{-\infty}^{\infty} P(\tilde{\boldsymbol{x}}, \omega) e^{i(\omega t - MK_1\tilde{x}_1)}\,\mathrm{d}\omega\right\} \qquad (2)$$

In the direct aeroacoustic problem, the far-field pressure is calculated using Eq. (1) when the unsteady pressure on the wing is known. In the inverse problem, Eq. (1) must be solved for the surface pressure in terms of the far-field pressure $P(\tilde{\boldsymbol{x}})$. Equation (1) is then a Fredholm integral equation of the first kind, requiring both the magnitude and relative phase of the far-field pressure to be measured/known. The integral equation is solved using the collocation method to obtain a matrix equation that is subsequently solved using algebraic techniques.

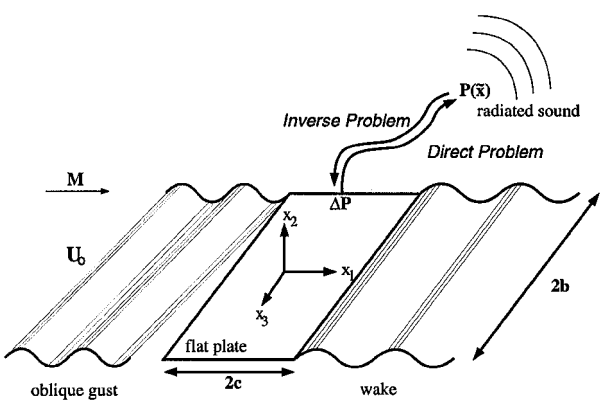

Fig. 1 Aeroacoustic considerations of a flat plate, rigid, rectangular wing in unsteady flow.

Matrix Representation of Integral Equation

The unsteady surface pressure jump ΔP is expressed as a linear combination of basis functions with unknown coefficients to be calculated. The basis functions are chosen in accord with common models in aerodynamics. A modified Fourier sine series is used in the streamwise direction; the sine series ensures that the Kutta condition is satisfied, and an additional term is added to the series to model the leading-edge suction. For the case of a vortical disturbance, the predominant chordwise behavior of the unsteady surface pressure jump that captures the leading edge suction is the Sears solution[12]:

$$\Delta P = 2\sqrt{(y_1 - 1)/(y_1 + 1)}\,\mathcal{S}(k_1) = 2i\cot(\theta/2)\mathcal{S}(k_1) \qquad (3)$$

where $\theta = \cos^{-1}(-\tilde{y}_1)$. For an oscillating wing and for an acoustic disturbance, the spatial variation of the predominant behavior is identical, but the frequency-dependent weighting function is different. Any differences in the weighting function can be absorbed by the unknown coefficient in the series, and thus, only the spatial variation is used in the series. Therefore, the representation of ΔP in the streamwise direction becomes

$$\Delta P = C_0(\tilde{y}_3, k_1)\cot\left(\frac{\theta}{2}\right) + \sum_{l=1}^{\infty} C_l(\tilde{y}_3, k_1)\sin(l\theta) \qquad (4)$$

The coefficients C_i are functions of the spanwise coordinate and account for variations arising from finite aspect ratio and oblique gust effects. Because the mean flow is not impinging on the sharp side edges of the wing, there are no singular suction peaks at the wing tips. For steady loading, downwash due to the finite aspect ratio effectively causes the maximum pressure jump to occur at the centerspan. This finite span model is adapted for unsteady loading using the following sinusoidal basis for the spanwise distribution:

$$C_j(\tilde{y}_3, k_1) = \sum_{n=1}^{\infty} B_{jn}(k_1)\sin(n\phi) \qquad (5)$$

where $\tilde{y}_3 = -\tilde{b}\cos\phi$. In Ref. 22, Eq. (4) was used with a complex exponential form for Eq. (5); the results of the present work show Eq. (5) to be a more suitable form.

The total unsteady surface pressure will be approximated by truncating the series in Eqs. (4) and (5) after L and N terms, respectively. One can then substitute Eqs. (4) and (5) into Eq. (1), integrate term by term, and evaluate the resulting expression in the far field ($\tilde{x} \gg 1$) to obtain the following expression for the transformed far-field acoustic pressure:

$$P(\tilde{\boldsymbol{x}}) = -\pi\hat{\tilde{x}}_2\left[iK_1 + \frac{1}{\tilde{x}}\right]\frac{e^{-iK_1\tilde{x}}}{\tilde{x}}\sum_{n=1}^{N} n(-i)^{n-1}\frac{J_n(K_1\tilde{b}\hat{\tilde{x}}_3)}{K_1\hat{\tilde{x}}_3}$$

$$\times\left[B_{on}(J_0(K_1\hat{\tilde{x}}_1) - iJ_1(K_1\hat{\tilde{x}}_1))\sum_{l=1}^{L} 2B_{ln}l(-i)^{l-1}\frac{J_l(K_1\hat{\tilde{x}}_1)}{K_1\hat{\tilde{x}}_1}\right] \tag{6}$$

The $(L+1)N$ unknowns B_{ln} are determined using $(L+1)N$ or more equations formed by applying Eq. (6) at points $\tilde{\boldsymbol{x}}$ in the far field surrounding the wing. The unknown coefficients are thus determined by solving the matrix system

$$\boldsymbol{p} = A\boldsymbol{b} \tag{7}$$

where $\boldsymbol{b}$ is a vector containing the unknown coefficients B_{ln} and A is the transfer matrix. Each row of the matrix equation (7) represents Eq. (6) at a particular location in the far field where the acoustic pressure is known.

Solution of the Matrix Equation

In practice, the number of far-field measurements will generally exceed the number necessary to perform the inversion. This produces an overdetermined system of equations that is typically solved by considering $A^T\boldsymbol{p} = A^TA\boldsymbol{b}$. However, as mentioned earlier, the matrix A is ill-conditioned, and a more sophisticated technique is required to obtain a solution when measurement and computational errors are present. The solution is obtained effectively by using the SVD method, which is briefly described here (see Ref. 24 for more details).

For a given complex-valued matrix $A \in \mathcal{C}_r^{m\times n}$, where r is the rank of A and $m \geq n \geq r$, two unitary matrices $U \in \mathcal{C}_r^{m\times m}$ and $V \in \mathcal{C}_r^{n\times n}$ exist such that

$$A = U\Sigma V^H \tag{8}$$

where

$$\Sigma = \begin{bmatrix} S & 0 \\ 0 & 0 \end{bmatrix}, \qquad S = \mathrm{diag}(\sigma_1, \ldots, \sigma_r), \qquad \sigma_1 \geq \cdots \geq \sigma_r > 0 \tag{9}$$

The SVD method defines the pseudoinverse of A such that the least-squares solution to Eq. (7) is given by

$$\boldsymbol{x} = V(\Sigma^+U^H\boldsymbol{p}) = V\boldsymbol{f}, \qquad \text{where} \qquad \Sigma^+ = \begin{bmatrix} S^{-1} & 0 \\ 0 & 0 \end{bmatrix} \tag{10}$$

The elements of $\boldsymbol{f} = \Sigma^+U^H\boldsymbol{p}$ will hereafter be referred to as the pseudoinverse coefficients. The SVD may be obtained numerically using standard algebraic routines, for example, LAPACK, IMSL, etc.

Application of the SVD and Regularization Techniques

The surface pressure is modeled using the collocation series [Eqs. (4) and (5)], which, from Fourier analysis, converges analytically. Thus, the series may be truncated after n terms to describe the solution within an acceptable level of accuracy. To have a completely determined system of equations for Eq. (7), m far-field measurement points must be chosen where $m \geq n$. Because of the series convergence, the last $n-r$ terms remaining in the truncated series may contribute relatively little to the solution compared to the preceding terms. The corresponding singular values, for example, σ_n, σ_{n-1}, etc., will be close to zero (relative to σ_1). The effect of numerical errors on the SVD causes these smaller contributions to be very poorly inverted. Therefore, the last $n-r$ singular values should be removed by defining them to be numerically zero, which is shown by the lower right submatrix in Eq. (9). The set of solutions defined by these $(\sigma_{r+1}, \ldots, \sigma_n)$ singular values will be referred to as the effective nullspace of A. The least-squares solution is then given by Eq. (10). Hereafter r will be referred to as the numerical rank of A.

For an ill-conditioned matrix, the numerical rank may not be clearly defined, and it may be difficult to determine which singular values are to be kept in the inversion and which are are to be discarded. Techniques that make this decision are termed regularization techniques. The simplest and most common method is the truncated SVD (TSVD), where a regularization parameter τ is defined such that all singular values falling below τ are set to zero. Here τ may be interpreted as the threshold for numerical zero and depends on both the numerical and measurement error in the problem. Another regularization technique commonly used is Tikhonov regularization,[25] where $S^+ = \mathrm{diag}[\sigma_i/(\sigma_i^2 + \tau); i = 1, \ldots, r]$ replaces S^{-1} in Eq. (10). This causes the singular values below the threshold parameter to be smoothly damped as opposed to the abrupt cutoff of the truncation scheme. However, neither the Tikhonov nor the simple truncation regularization methods work well for the present problem because variations in the physical parameters (flow speed, frequency, etc.) produce significant variations in the value of the cutoff τ required for accurate reconstruction of the surface pressure (see Fig. 3 in Ref. 23).

Diagnosing an Optimal Reconstruction

The solution of the matrix equation (7) for the coefficients $\boldsymbol{b}$ depends on the physical flow parameters k_1, M, and k_3, and the measured far-field pressure. Because the inverse problem defined by Eq. (6) is ill-conditioned, the solution for B_{ln} becomes increasingly inaccurate for higher l and n in the presence of numerical and measurement errors. There exists, however, an optimal choice of the truncation indices L and N such that the solution converges as the number of terms used in the series for ΔP increase up to $(L+1)N$, and the solution diverges as the number of terms increase beyond. The resulting solution for the surface pressure using the optimal series length given by the set $\{L, N\}$ will be referred to as the semi-converged solution. The ability to determine the optimal numerical basis for a given set of far-field pressure measurements and flow parameters will determine the quality of the surface pressure reconstruction. When the optimal set of truncation indices is used, a regularized system is obtained, and the inverse may be calculated without spectral truncation or regularization.

The terms in the collocation series for ΔP are ordered (approximately) by their relative importance; hence, the pressure distribution is determined predominantly by the first few terms of the series. Thus, one may start with an overtruncated system using, for example, the first two terms in each series, which is normally insufficient to describe accurately the unsteady surface pressure distribution. The next higher term may then be iteratively included until divergence occurs, indicating that the numerical rank has been determined and the singular values that are numerically zero have been identified.

Consideration of the pseudoinverse coefficients, $\boldsymbol{f} = \Sigma^{-1}U^H\boldsymbol{p}$, provides a more transparent indication of an ignorable contribution when compared to the traditional regularization techniques. Because the columns $\{\boldsymbol{v}_i\}$ of V form an orthonormal basis for the solution vector $\boldsymbol{b}$, the magnitude of f_i determines the relative contribution of the ith vector to the optimal solution. Singular values that are exactly zero correspond to a coefficient that is infinite; a singular value σ_i will be numerically zero only when it is small compared to $\boldsymbol{u}_i \cdot \boldsymbol{p}$ such that f_i attains unphysically high magnitudes. Note that $\boldsymbol{u}_i \cdot \boldsymbol{p}$ could be as small as σ_i such that $\boldsymbol{u}_i \cdot \boldsymbol{p}/\sigma_i$ is finite, which indicates a necessary contribution of the ith term to the inverse solution. As compared to the currently used regularization techniques, use of the pseudoinverse coefficients to truncate the collocation series permits a clearer and more precise determination of the numerical rank of the matrix at no extra computational expense. The advantages are clear because traditional regularization methods assume the singular values are a measure of the relative contributions of each term, irrespective of the interaction with the far-field measurements. Hence, two singular values (from two independent SVDs) of equal magnitude can represent radically different contributions to the inverse solution, namely, a physical and a nullspace contribution. However, the proposed method can distinguish these two extremes because the corresponding pseudoinverse coefficients would be quite different.

Statement of Algorithm

An algorithm for automatic calculation of the optimal solution to the inverse problem may now be formulated explicitly. One begins with an overtruncated series [i.e., L and N in Eq. (6) sufficiently small] and performs the SVD to calculate the coefficients $\boldsymbol{f}$. Because the unknown surface pressure is overapproximated, that is, the truncation error of the collocation series is high, the last coefficient will be relatively large, and thus, it represents an essential contribution. The value of L or N is then increased in steps until an adequate approximation to the solution is achieved, which occurs when the last pseudoinverse coefficient, f_E $[E = (L + 1)N]$, is a small fraction of the first (fundamental) coefficient f_1 and less than the previous coefficient f_{E-1}. Once this first approximation is achieved, the truncation error of the series in Eqs. (4) and (5) may be reduced by increasing the truncation indices L and N until the effect of ill-conditioning causes the series to appear to diverge. Hence, the optimal solution is obtained from the first approximation by increasing L by 1 and applying the test

$$(f_E < \alpha f_1), \qquad (f_E < f_{E-1}) \tag{11}$$

where $\alpha < 1$ and should be typically around 10%. The value of L is then repeatedly increased while the condition in Eq. (11) is satisfied. When the condition fails, N is increased by 1 and the preceding steps are repeated until a state is found where Eq. (11) is true for $\{L, N\}$ yet fails for both $\{L + 1, N\}$ and $\{L, N + 1\}$. The optimal reconstruction of the unsteady, nondimensional, transformed surface pressure is then determined by forming the matrix equation (7) using the optimal set (L, N), solving for the unknown coefficients using

$$\boldsymbol{b} = A^{+}\boldsymbol{p} = V\boldsymbol{f} \tag{12}$$

and substituting the coefficients into the series representation of ΔP given by Eqs. (4) and (5).

In certain instances, the second condition in Eq. (11) must be amended to consider coefficients preceding f_{E-1}. When the incident gust is parallel to the leading edge ($k_3 = 0$), the surface pressure distribution is symmetric about the centerspan of the wing. As a result, all of the even terms in Eq. (5) will not contribute and will yield pseudoinverse coefficients that are zero. In this case, the comparison to $f_E < f_{E-2}$ may be made instead of that given in Eq. (11), or the even terms in Eq. (5) may be removed before performing the SVD.

Note on Far-Field Data

To test the commonly used regularization methods, numerically generated far-field data for a vortical gust interacting with the wing [using the direct integration of Eq. (1)] were used.[18] The streamwise variation of the surface pressure was taken to be Possio's solution for an airfoil in a two-dimensional, compressible fluid interacting with an oblique gust.[11] Prandtl's lifting-line theory was then employed as a simple test model of the spanwise variation of the surface pressure for finite aspect ratio effects.[26] A sinusoidal variation given by $\exp(ik_3\tilde{x}_3)$, where k_3 is the spanwise wave number component, is then imposed. The far-field measurements were sampled on a spherical surface centered on the center of the wing. By sampling at equal increments of ϑ (measured from the x_3 axis) and φ (measured from the x_1 axis, see Fig. 2) the set of numerically generated far-field measurements:

$$P_{cd} = \{(r, \vartheta_c, \varphi_d) : c = 1, \ldots, C; d = 1, \ldots, D\} \tag{13}$$

is obtained, where $CD \geq (L + 1)N$ in order for the system to be completely determined. For flow parameters of interest, no more than about 40 measurements need be taken to satisfy this requirement. In the majority of cases, however, more data will be taken than required. These extra data are useful when measurement error is present because the solution method just described performs a least-squares fit. For all of the results presented in this paper, $C = 5$ and $D = 41$ were chosen (arbitrarily) for the measurement set in Eq. (13). Note that no optimization of the measurement locations was performed in this research; however, changes in the measurement locations can increase the accuracy of the inverse solution by reducing the level of ill-conditioning in the matrix A (Ref. 27).

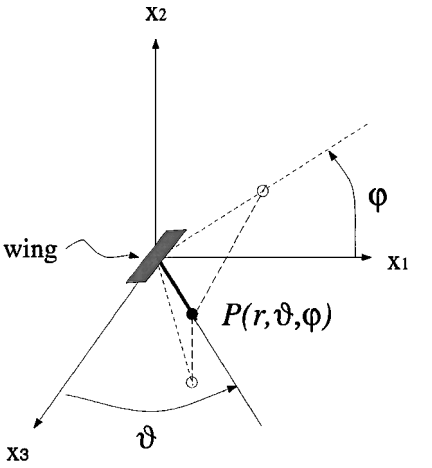

Fig. 2 Definition of spherical coordinate system used in the far field.

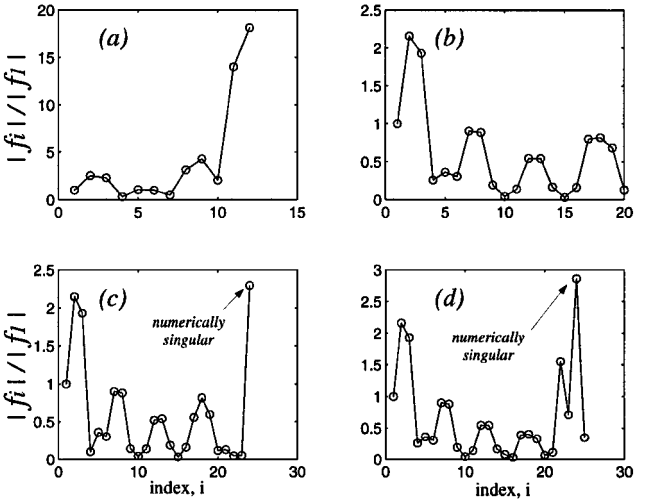

Fig. 3 Pseudoinverse coefficient magnitudes $|f_i|$ for $\gamma = 0.2$ ($k_1 = 3$, $M = 0.3$) normalized by $|f_1|$: a) overtruncated series, b) optimally truncated series, c) appearance of nullspace because of inclusion of noninvertible spanwise contribution, and d) appearance of nullspace because of inclusion of noninvertible streamwise contribution.

Results

As already mentioned, the pseudoinverse coefficients provide a more effective means of determining the numerical rank of an ill-conditioned matrix. In Fig. 3, the magnitudes of f_i are shown relative to that of f_1 for four different truncated series for an obliquely incident gust in low Mach number flow. Series b is the semiconverged solution, which yields a good reconstruction using all of the singular values (Fig. 3b). Series c and d (Figs. 3c and 3d) are obtained by adding the $(L + 1)$th and $(N + 1)$th terms, respectively, to series b. In these cases, $\boldsymbol{f}$ becomes very large and, thus, indicates that the corresponding singular value is numerically zero. Hence, the corresponding singular vector may be treated as a nullspace contribution, and the numerical rank of the matrix is the number of terms in series b. Figure 3a shows the result for the case when the approximation series is highly overtruncated. Here the basis is deficient in spanning the solution, and the computation reacts by overweighting the last few singular vectors. In this situation, the number of terms in the series must be increased to render an adequately approximated solution; that is, this pattern should not be confused with the appearance of a nullspace. Through consideration of the pseudoinverse coefficients, the inverse solution is amenable to automatic calculation by using a pattern recognition computer scheme. Typical comparisons between surface pressure reconstructions made using the present technique and the standard TSVD (see Fig. 5 of Ref. 23) demonstrate the effectiveness of the new regularization technique.

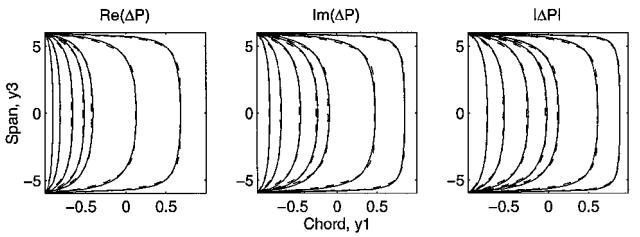

$k_1 = 3.0, M = 0.1$

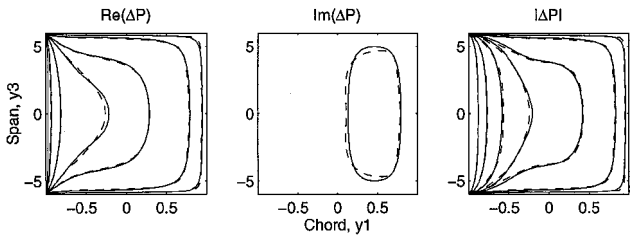

$k_1 = 5.0, M = 0.3$

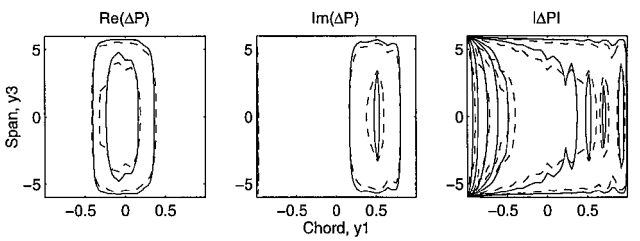

$k_1 = 7.0, M = 0.8$

Fig. 4 Inverse solutions for a parallel gust ($k_3 = 0$): ——, exact model, and - - - -, inverse solution.

Inverse Solutions

The proposed solution algorithm has been used to calculate the inverse solutions for a variety of cases. Reduced frequencies ranging from 1 to 7 and Mach numbers from 0.1 to 0.8 are considered for oblique gusts ($k_3 \neq 0$) constituting up to 80% cutoff [$\gamma = 0.8$, where γ is defined such that $\sqrt{(K_1^2 - k_3^2/\beta^2)} = (1-\gamma)K_1$]; note that cutoff refers to cases where k_3 is high enough to yield acoustic cutoff for the two-dimensional (infinite aspect ratio) case.[21] Only wings with an aspect ratio equal to 6 were used, and all of the far-field measurements were made on a hemisphere with a radius of 100 half-chord lengths centered on the wing. Figure 4 presents results for parallel gusts ($k_3 = 0$). Excellent reconstructions of the unsteady surface pressure are obtained for relatively low Mach numbers and low frequencies ($K_1 < 2$). As the disturbance frequency k_1 and/or the Mach number increase, a decrease in the accuracy of the inverse solutions is observed. Figure 5 presents a result for varying k_3. The spanwise variations are shown in the real and imaginary parts of the surface pressure jump, whereas the magnitude of ΔP is equivalent to the parallel gust case due to the $\exp(ik_3\tilde{x}_3)$ variation.

A quantitative measure of the relative errors between the inverse solutions and the input models was calculated for several cases, and the results are summarized in Table 1. The error is calculated using

$$\epsilon = \frac{\Sigma_i [p_{\text{calculated}}(\boldsymbol{x}_i) - p_{\text{model}}(\boldsymbol{x}_i)]^2}{\Sigma_i [p_{\text{model}}(\boldsymbol{x}_i)]^2} \tag{14}$$

where p is either the surface pressure jump (near field) or the acoustic pressure at the measurement surface (far field) and $\boldsymbol{x}_i$ is the corresponding spatial coordinate of the ith point. The calculated far-field pressure is obtained by performing the direct integration of the inverse solution. One can see from Table 1 a general trend of increased error with increased K_1. The error in the reconstruction of $M = 0.1$ ($k_3 = 0$) is approximately 0.06%. An increase in K_1 by a factor of 3.26 ($M = 0.3$) yields about a 0.1% increase in the reconstruction error; a factor of 9.28 increase in K_1 ($M = 0.6$) results in an error that is 1% greater. Note that, in some cases, the error is reduced for increased k_3 while K_1 remains fixed; $\gamma = 0.5$ and 0.8 for

Table 1 Error of reconstructions relative to input models

k_1	Mach	K_1	γ	k_3	Near-field error	Repropagated far-field error
3.0	0.1	0.3030	0.0	0.0000	$6.45E-04$	$3.16E-10$
3.0	0.1	0.3030	0.2	0.1809	$2.74E-03$	$3.40E-10$
3.0	0.1	0.3030	0.5	0.2611	$5.83E-04$	$5.11E-11$
3.0	0.1	0.3030	0.8	0.2954	$6.07E-04$	$2.03E-12$
3.0	0.3	0.9890	0.0	0.0000	$1.71E-03$	$2.85E-12$
3.0	0.3	0.9890	0.2	0.5661	$4.69E-03$	$5.52E-11$
3.0	0.3	0.9890	0.5	0.8171	$1.94E-03$	$2.04E-11$
3.0	0.3	0.9890	0.8	0.9244	$4.38E-03$	$2.15E-11$
5.0	0.3	1.6484	0.0	0.0000	$3.93E-03$	$1.23E-09$
7.0	0.3	2.3077	0.0	0.0000	$6.22E-03$	$9.45E-08$
3.0	0.6	2.8125	0.0	0.0000	$1.15E-02$	$2.99E-04$
3.0	0.6	2.8125	0.2	1.3500	$3.52E-01$	$6.10E-04$
3.0	0.6	2.8125	0.5	1.9486	$1.87E-01$	$1.61E-05$
3.0	0.6	2.8125	0.8	2.2045	$7.64E-02$	$1.10E-09$
5.0	0.6	4.6875	0.0	0.0000	$1.62E-02$	$3.31E-04$
7.0	0.6	6.5625	0.0	0.0000	$3.62E-02$	$2.13E-04$
3.0	0.8	6.6667	0.0	0.0000	$4.52E-02$	$5.23E-04$
5.0	0.8	11.1111	0.0	0.0000	$6.40E-02$	$1.52E-04$
7.0	0.8	15.5556	0.0	0.0000	$9.17E-02$	$9.67E-05$

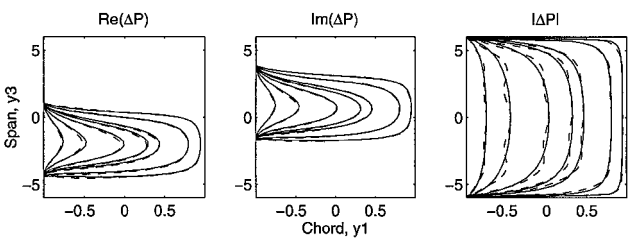

$k_3 = 0.5661$

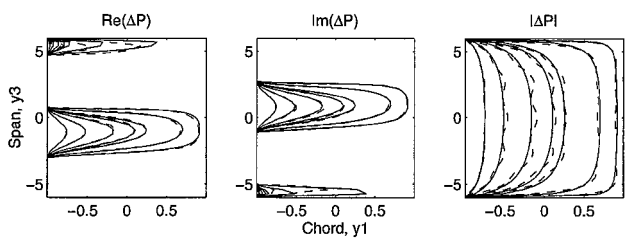

$k_3 = 0.8171$

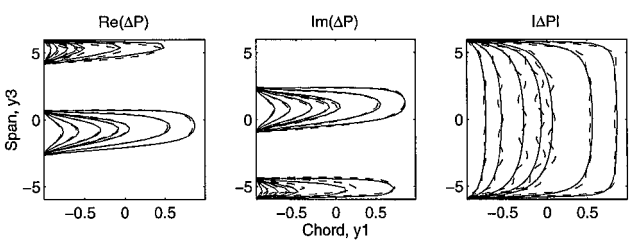

$k_3 = 0.9244$

Fig. 5 Inverse solutions for an oblique gust ($k_1 = 3$, $M = 0.3$): ——, exact model, and - - - -, inverse solution.

$K_1 = 0.303$ result in a 0.006 and 0.004% reduction in error, respectively (relative to $\gamma = 0$). This reduces the number of streamwise terms required in the approximation series and, thus, increases the accuracy of the inverse solution if the number of spanwise terms remains relatively low. However, as the spanwise variation increases (as seen for $K_1 = 0.989$ and 2.81), more terms in the spanwise collocation series will be required, and the reconstruction error will increase because of ill-conditioning.

Effect of Input Error

The results of the preceding sections used six-digit accuracy in the input data. By reducing the number of significant figures retained

in the input data, a biased random error is simulated. The resulting pressure distribution for $M = 0.6$ and $k_1 = 3.0$ using only one significant figure is shown in Figs. 6 and 7. The inverse solution is such that the repropagated far field will fit to a smoothed input distribution because the highly varying contributions associated with random noise are noninvertible due to the ill-conditioning and are not computed in the inverse solution.

The effect of adding uniform random noise (zero mean, constant probability density on the interval $[x(1-\epsilon), x(1+\epsilon)]$, where ϵ is the maximum error) to both the magnitude and phase of the input data is summarized in Table 2. The general trend is an increase in reconstruction error with increased input error. An increase from 1 to 10% in the maximum error leads to an increase of reconstruction error by 0.5% for the $M = 0.1$ case. For $M = 0.6$ with 25% input error, the collocation series must be truncated to three streamwise terms and one spanwise term [as determined by the pseudoinverse coefficient test; Eq. (11)] to obtain the optimal surface pressure reconstruction. Eventually as the input error increases, no truncated collocation series will result in an optimal reconstruction as defined using the pseudoinverse coefficients.

The inverse solution also requires the mean flow Mach number and the frequency of the disturbance as input to the calculation. All of the preceding results have been calculated using double-precision accuracy for both of these quantities. In Tables 3 and 4, the errors in the reconstructions are given for varying fractional error in k_1 and M, respectively. Errors in either k_1 or M affect the Helmholtz parameter, $K_1 = k_1 M/\beta^2$, primarily. Hence, both quantities have similar sensitivities to error, with the reconstructions being slightly more sensitive to the Mach number because of the $\exp(-iMK_1\bar{x}_1)$ term that appears in Eq. (2). Inverse solutions for the unsteady near-field pressure can be obtained for errors in K_1 up to approximately 10%, for highly accurate far-field data. For high error in k_1 or M, the phase of the reconstructed field becomes much more inaccurate than the magnitude, as shown in Fig. 8. This occurs when the collocation series is truncated to only one term in the streamwise expansion. The resulting error in the magnitude of the surface pressure

Table 2 Effect of input error[a] ($k_1 = 3.0$)

Mach	Input error, %	Reconstruction error	Repropagated far-field error
0.1	0.01	0.001	1.15E−07
0.1	0.10	0.004	3.07E−05
0.1	1.00	0.014	1.40E−03
0.1	5.00	0.015	3.32E−02
0.1	10.00	0.020	1.24E−01
0.1	25.00	0.174	5.86E−01
0.6	0.01	0.011	2.99E−04
0.6	0.10	0.012	3.11E−04
0.6	1.00	0.042	1.43E−03
0.6	5.00	0.058	3.40E−02
0.6	10.00	0.077	9.07E−02
0.6	25.00	0.204	5.36E−01

[a]Input error represents the maximum error (uniform noise distribution) added to both the magnitude and phase (independently) of the input measurements.

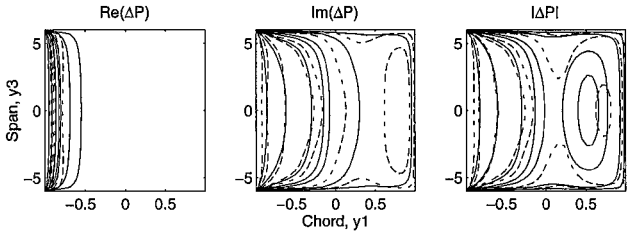

Fig. 6 Inverse solution for $k_1 = 3$, $M = 0.6$, and $k_3 = 0$; input data used are accurate to one significant figure: ——, exact model, and - - - -, inverse solution.

Table 3 Effect of k_1 error for the case $k_1 = 3$, $M = 0.1$, $\gamma = 0$

Error in k_1	Reconstruction error	Repropagated far-field error
0.0001	5.93305E−04	2.13175E−10
0.0010	1.30267E−03	1.17699E−09
0.0100	1.31486E−01	2.66123E−07
0.0500	6.81150E−01	1.83228E−05
0.1000	7.75194E−01	1.55639E−02

Table 4 Effect of M error for the case $k_1 = 3$, $M = 0.1$, $\gamma = 0$

Error in M	Reconstruction error	Repropagated far-field error
0.0001	4.47322E−04	2.05566E−10
0.0010	1.83439E−03	5.04308E−09
0.0100	2.51849E−01	1.36329E−06
0.0500	2.88402E−01	1.82842E−04
0.1000	6.99769E−01	7.07353E−02

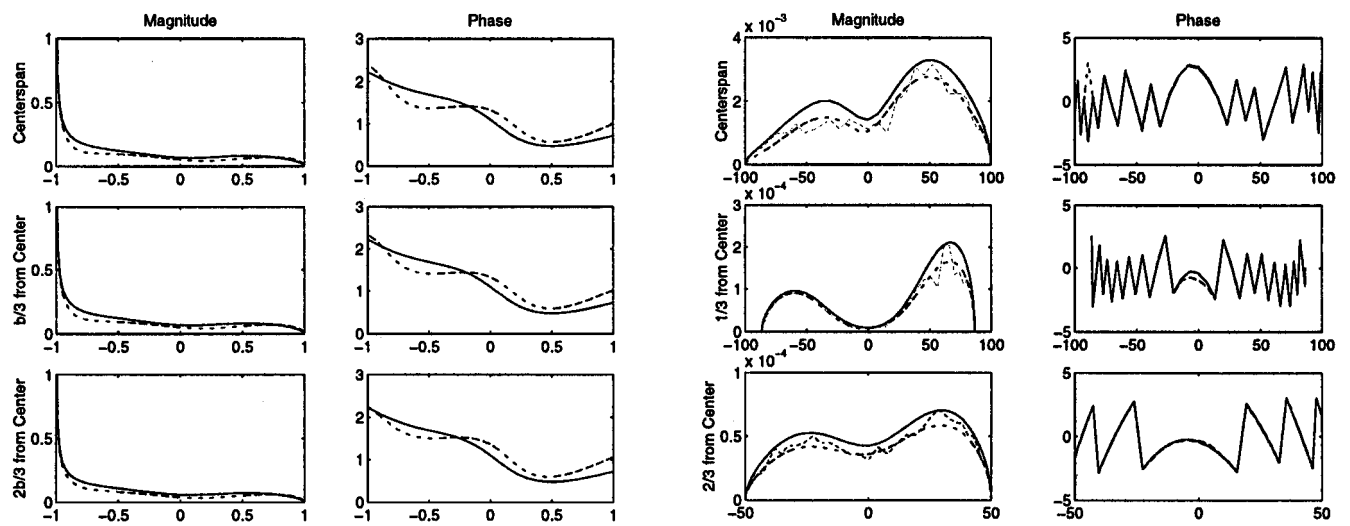

Fig. 7 Streamwise cross-sectional views for $k_1 = 3$, $M = 0.6$, and $k_3 = 0$, using one digit accuracy in the input data: ——, input model; - - - -, inverse solution; and · · · ·, far-field data with error.

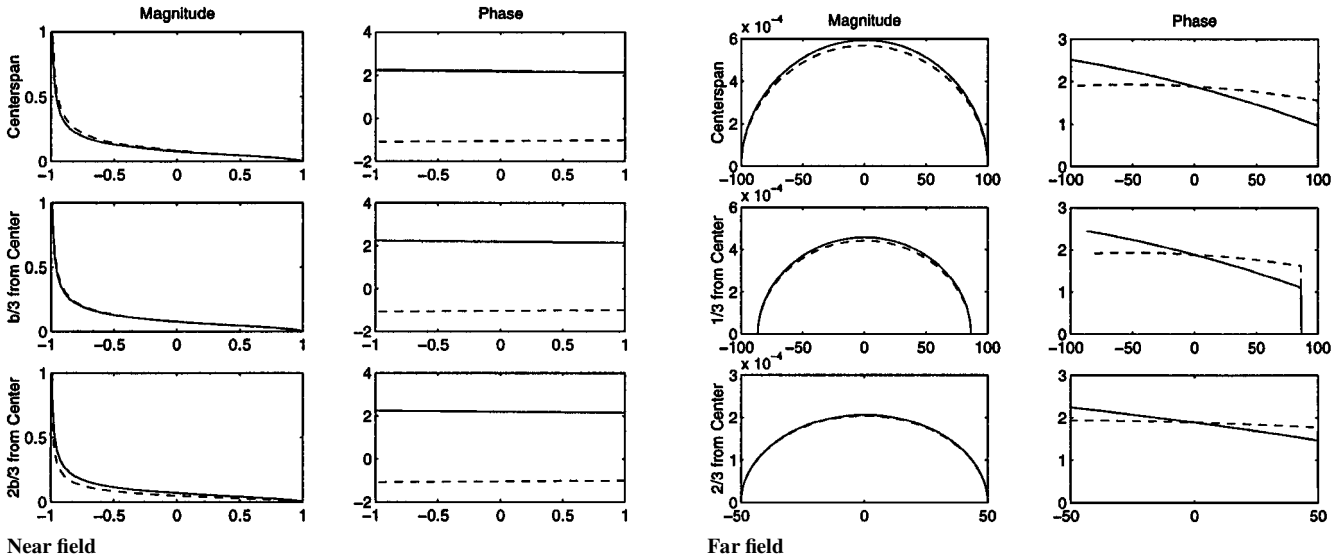

Fig. 8 Streamwise cross-sectional views for $k_1 = 3$, $M = 0.1$, and $\gamma = 0$, using 0.977% error in M, such that the error in K_1 is 1%: ——, input model, and - - - -, inverse solution.

reconstruction for a 10% deviation in k_1 is 2.5% (cf., total error, in magnitude and phase, of 78% in Table 3).

Conclusions

This research demonstrates the feasibility of the three-dimensional aeroacoustic inverse problem for a flat-plate, rectangular wing in weakly unsteady, inviscid, subsonic flow and develops the techniques required to allow for a practical implementation of the method. The method for reconstruction of the unsteady surface pressure has been validated using obliquely incident vortical gusts of moderate frequencies in subsonic flow (K_1 up to approximately 10). Approximately 25% error in the input data or 10% error in the input flow parameters can be accommodated with adequate results. Although the reconstructions are more sensitive to errors in the input parameters than in the field data, the magnitude of the surface pressure is reconstructed very accurately (errors below 2.5%) for deviations in K_1 up to 10%; however, errors in the phase of the reconstructed unsteady surface become very high for K_1 deviations greater than approximately 5%.

The three-dimensional inverse aeroacoustic problem hinges on the solution to an ill-conditioned matrix equation arising due to the ill-posedness of the problem. Existing regularization techniques for solving the ill-conditioned systems of equations were not effective because of their need for an a priori regularization parameter, which was shown to vary dramatically with the flow parameters. Therefore, a new regularization method for use with the SVD has been developed. The current method uses the coefficient vector of the pseudoinverse solution instead of the singular values to calculate the solution through regularization. This gives an added ease and adaptability in using the inversion method for practical applications.

The feasibility of the inverse aeroacoustic problem as shown in this research is dependent on the assumption of uniform mean flow. The method may have to be amended to account for a nonuniform mean flow (i.e., real wing geometries) and freestream turbulence (which has a significant noise contribution at near sonic Mach numbers). This must be the focus of future research.

Acknowledgment

T. Wood would like to thank the Natural Sciences and Engineering Research Council of Canada for providing PGS B funding for this project.

References

[1]Sleeman, B. D., "The Three-Dimensional Inverse Scattering Problem for the Helmholtz Equation," *Proceedings of the Cambridge Philosophical Society*, 1973, pp. 477–488.

[2]Maynard, J. D., Williams, E., and Lee, Y., "Nearfield Acoustic Holography: I. Theory of Generalized Holography and the Development of NAH," *Journal of the Acoustical Society of America*, Vol. 78, No. 4, 1985, pp. 1395–1412.

[3]Veronesi, W. A., and Maynard, J. D., "Digital Holographic Reconstruction of Sources with Arbitrarily Shaped Surfaces," *Journal of the Acoustical Society of America*, Vol. 85, No. 2, 1989, pp. 588–598.

[4]Meadows, K. R., Brooks, T. F., Humphreys, W. M., Hunter, W. H., and Gerhold, C. H., "Aeroacoustics Measurements of a Wing-Flap Configuration," AIAA Paper 97-1595, May 1997.

[5]Dougherty, R. P., and Stoker, R. W., "Sidelobe Suppression for Phased Array Aeroacoustic Measurements," *Proceedings of the AIAA/CEAS 4th Aeroacoustics Conference*, AIAA, Reston, VA, 1998, pp. 235–245.

[6]Humphreys, W. M., Brooks, T. F., Hunter, W. H., and Meadows, K. R., "Design and Use of Microphone Directional Arrays for Aeroacoustic Measurements," AIAA Paper 98-0471, June 1998.

[7]Brooks, T. F., and Humphreys, W. M., "Effect of Directional Array Size on the Measurement of Airframe Noise Components," AIAA Paper 99-1958, May 1999.

[8]Michel, U., Barsikow, B., Helbig, J., Hellmig, M., and Schüttpelz, M., "Flyover Noise Measurements on Landing Aircraft with a Microphone Array," AIAA Paper 98-2336, June 1998.

[9]Michel, U., and Qiao, W., "Directivity of Landing-Gear Noise Based on Flyover Measurements," AIAA Paper 99-1956, May 1999.

[10]Theodorsen, T., "General Theory of Aerodynamic Instability and the Mechanism of Flutter," NACA-TR-496, 1949, pp. 413–433.

[11]Graham, J. M. R., "Similarity Rules for Thin Airfoils in Non-Stationary Subsonic Flows," *Journal of Fluid Mechanics*, Vol. 43, No. 4, 1970, pp. 753–766.

[12]Sears, W. R., "Some Aspects of Non-Stationary Airfoil Theory and Its Practical Application," *Journal of Aeronautical Sciences*, Vol. 8, No. 3, 1941, pp. 104–108.

[13]Possio, C., "L'Azione Aerodinamica sul Prodilo Oscillante in un Fluido Compressible a Velocita Ipsonora," *L'Aerotecnica*, Vol. 28, Fasc. 4, 1938.

[14]Adamczyk, J. J., "Passage of a Swept Airfoil Through an Oblique Gust," *Journal of Aircraft*, Vol. 11, No. 5, 1974, pp. 281–287.

[15]Howe, M. S., "The Influence of Vortex Shedding on the Generation of Sound by Convected Turbulence," *Journal of Fluid Mechanics*, Vol. 76, 1976, pp. 711–740.

[16]Martinez, R., and Widnall, S. E., "Unified Aerodynamic-Acoustic Theory for a Thin Rectangular Wing Encountering a Gust," *AIAA Journal*, Vol. 18, No. 5, 1980, pp. 636–645.

[17]Amiet, R. K., "Acoustic Radiation from an Airfoil in a Turbulent Stream," *Journal of Sound and Vibration*, Vol. 41, No. 4, 1975, pp. 407–420.

[18]Atassi, H. M., Dusey, M., and Davis, C. M., "Acoustic Radiation from a Thin Airfoil in Nonuniform Subsonic Flow," *AIAA Journal*, Vol. 31, No. 1, 1993, pp. 12–19.

[19]Epstein, R. J., and Bliss, D. B., "Aeroacoustic Boundary Element Method Using Analytical/Numerical Matching," *AIAA Journal*, Vol. 35, No. 2, 1997, pp. 244–254.

[20]Patrick, S. M., "An Inverse Problem for a Nonuniform Subsonic Flow Interacting with a Body and Radiating Sound," Ph.D. Thesis, Dept. of Aerospace and Mechanical Engineering, Univ. of Notre Dame, Notre Dame, IN, April 1995.

[21]Patrick Grace, S., Atassi, H. M., and Blake, W. K., "Inverse Aeroacoustic Problem for a Streamlined Body Part 1: Basic Formulation," *AIAA Journal*, Vol. 34, No. 11, 1996, pp. 2233–2240.

[22]Patrick, S. M., and Atassi, H. M., "Inverse Aeroacoustic Problem for a Rectangular Wing Interacting with a Gust," AIAA Paper 96-1790, May 1996.

[23]Wood, T. H., and Grace, S. M., "Inverse Aeroacoustic Problem for a Rectangular Wing in a Gust," *Proceedings of the AIAA/CEAS 4th Aeroacoustics Conference*, AIAA, Reston, VA, 1998, pp. 162–173.

[24]Golub, G. H., and van Loan, C. F., *Matrix Computation*, 3rd ed., Johns Hopkins Univ. Press, Baltimore, MD, 1989, pp. 69–75, 253–258.

[25]Tikhonov, A. N., "Regularization and Incorrectly Posed Problems," *Soviet Mathematics*, Vol. 4, No. 6, 1963, pp. 1624–1627 (English translation).

[26]Katz, J., and Plotkin, A., *Low-Speed Aerodynamics*, McGraw–Hill, New York, 1991, pp. 193–212.

[27]Yoon, S. H., and Nelson, P. A., "Reconstruction of Aeroacoustic Source Strength Distributions by Inverse Techniques," *Proceedings of the AIAA/CEAS 4th Aeroacoustics Conference*, AIAA, Reston, VA, 1998, pp. 783–793.

A. Plotkin
Associate Editor